Int. J. Heat Mass Transfer. Vol. 35, No. 10, pp. 2739–2749, 1992
Printed in Great Britain

0017–9310/92 $5.00 + 0.00

Viscous heating of a cylinder with finite length by a high viscosity fluid in steady longitudinal flow—II. Non-Newtonian Carreau model fluids

J. N. SHADID
Sandia National Laboratories, Parallel Computational Science Division, Albuquerque, NM 87185, U.S.A.

and

E. R. G. ECKERT
Department of Mechanical Engineering, University of Minnesota, Minneapolis, MN 55455, U.S.A.

(*Received* 24 *September* 1990 *and in final form* 29 *August* 1991)

Abstract—The viscous dissipation heating of a finite length cylinder exposed to a steady uniform velocity non-Newtonian fluid has been analyzed numerically. The solution determines the elliptic, velocity and temperature fields of a high viscosity non-Newtonian Carreau model fluid about an axisymmetric cylinder. With polymer processing in mind, Part I of this study [E. R. G. Eckert and J. N. Shadid, *Int. J. Heat Mass Transfer* **32**, 321–334 (1989)] considered the effect of the Reynolds number, Prandtl number, probe radius to length ratio and the ratio of cylinder conductivity to fluid thermal conductivity. This paper extends these results by considering the effect of a temperature-dependent non-Newtonian shear thinning viscosity modeled by a temperature shifted Carreau fluid. Computations were performed for different values of the power law exponent, the Weisenberg number, and the Nahme number. In this study calculations are presented for an adiabatic probe with a radius to length ratio of 2.5×10^{-2}, with the Reynolds and Prandtl numbers taken to be fixed at 10^{-3} and 10^{8} respectively. The power law exponent is varied from 1.0 (Newtonian) to 0.2, the Weisenberg number varies from 0 (Newtonian) to 10^{4}, and the Nahme number between 0 and 10^{4}. The results determine the increase in the cylinder wall and tip temperature due to viscous frictional heating. Strong elliptic effects on the velocity extend over 100 radius lengths upstream from the cylinder. As expected the shear thinning behavior of the non-Newtonian viscosity is found to decrease the magnitude of the viscous dissipation heating of the probe surface. In contrast, the effect of the temperature dependence of viscosity described by the Nahme number is found to have a relatively small influence on the cylinder tip temperature.

INTRODUCTION

In the flow of polymeric fluids, evaluation of the local temperature field is often of primary interest since a number of physical properties can vary substantially with temperature. In addition, relaxation phenomena in polymers are strongly temperature dependent, and the amount and location of residual stress or strain in the product will depend on the local temperature history of the polymer [1]. For this reason the temperature field can have a significant effect on the flow field as well as on the process itself.

The effort to measure local temperatures in a flowing polymer encounters the difficulty that any object exposed to a viscous flow is heated by internal friction in a process which converts mechanical energy in the fluid into internal energy and thus raises the probe temperature. This process is known as viscous heating. The resulting temperature increase has to be minimized or has to be determined by calibration if one wants to obtain from the recorded probe temperature the temperature which the fluid would have when the probe is absent.

The present paper reports the results of an analysis of viscous heating of a cylinder with finite length oriented with its axis parallel to the velocity of the oncoming non-Newtonian fluid flow. It is thought that the cylinder approximates the shape of a temperature probe inserted into the fluid. The velocity and temperature fields are obtained by the analysis, in addition to the surface temperature of the cylinder. Knowledge of these fields is a prerequisite to an understanding of the relation between the temperature history of a polymer melt and its effect on the macroscopic physical properties of the polymer material. Part I of this study [2] considered the effect of the Reynolds number, Prandtl number, probe radius to length ratio and the ratio of cylinder conductivity to fluid thermal conductivity. The results indicated a substantial increase in the cylinder wall and tip temperature due to viscous frictional heating. Strong elliptic effects on velocity were found to extend over 100

NOMENCLATURE

a_T temperature shift factor for viscosity, equation (13)
c_p^* specific heat
$\mathbf{D}^* = \frac{1}{2}(\nabla\mathbf{V}^* + \nabla\mathbf{V}^{*T})$ deformation rate tensor
E^* activation energy parameter in Arrhenius model, equation (14)
k^* thermal conductivity
L^* cylinder length
P^* pressure
$P = P^*R^*/\eta^*U_0^*$ dimensionless pressure
R^* cylinder radius
$\tilde{R}^*$ gas constant in Arrhenius model, equation (14)
r^* coordinate
$r = r^*/R^*$ dimensionless coordinate
T^* temperature
T_0^* upstream temperature
U_0^* upstream velocity
u^* velocity component
$u = u^*/U_0^*$ dimensionless velocity component
$\mathbf{V}^*$ velocity vector
v^* velocity component
$v = v^*/U_0^*$ dimensionless velocity component
x^* coordinate measured from cylinder tip
x_c^* coordinate measured from cylinder midplane
$x = x^*/R^*$ dimensionless coordinate.

Greek symbols
$\dot{\gamma}^*$ magnitude of deformation rate tensor $\mathbf{D}^*$, equation (13)
η^* viscosity
θ angular coordinate
$\Theta = (T^* - T_0^*)/(\eta^*U_0^*/\rho^*c_p^*R^*)$ nondimensional temperature
λ_p^* relaxation time parameter for Carreau model, equation (13)
ρ^* density
Φ^* dissipation function (see equation (6))
$\nabla\mathbf{V}^*$ velocity gradient tensor.

Dimensionless quantities
$Na = (\eta_0^*(E^*/\tilde{R}^*T_0^{*-1})U_0^{*2})/k^*$ Nahme number
$Pr = \eta^*c_p^*/k_f^*$ Prandtl number
$Re = 2\rho^*U_0^*R^*/\eta^*$ Reynolds number
$Wb = \lambda_p^*U_0^*/R^*$ Weisenberg number.

Superscripts
* dimensional quantity
T transpose.

Subscripts
0 upstream
f fluid
s solid
p cylinder tip.

radius lengths upstream from the cylinder. The velocity field results also indicated a nearly 'creeping flow' type velocity distribution about the cylinder body. In contrast, the temperature field was found to be confined to a very narrow region of high deformation rates around the cylinder surface. This study extends these results by considering the effect of a shear thinning, temperature-dependent non-Newtonian viscosity modeled by a temperature shifted Carreau fluid.

This paper, to our knowledge, presents the first study of this kind for an external flow around an object, whereas internal flow situations for pipes, ducts and extruders have been reported in the literature [1, 3].

PROBLEM FORMULATION

Conservation equations

The following equations describe the steady, laminar axisymmetric flow of a Carreau model non-Newtonian fluid past a cylinder arranged with its axis parallel to the main flow direction (Fig. 1). In the equations, the pressure work term in the energy equation and the gravity term in the momentum equation have been neglected. The equations have been made dimensionless by the following change of variables:

$$(x, r, u, v, P, \Theta, \eta) = \left(\frac{x^*}{R^*}, \frac{r^*}{R^*}, \frac{u^*}{U_0^*}, \frac{v^*}{U_0^*}, \frac{P^*R^*}{\eta^*U_0^*}, \frac{T^* - T_0^*}{\eta^*U_0^*/\rho^*c_p^*R^*}, \frac{\eta^*}{\eta_0^*}\right). \quad (1)$$

The symbols are defined in the Nomenclature and are also indicated in Fig. 1. The resulting dimensionless equations are:

Continuity equation

$$\frac{1}{r}\frac{\partial(rv)}{\partial r} + \frac{\partial u}{\partial x} = 0 \quad (2)$$

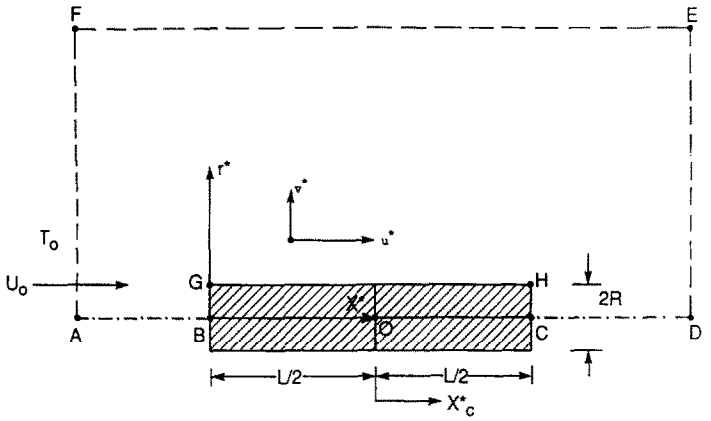

FIG. 1. Coordinate system and computational domain (not to scale).

Equations of motion

$$\tfrac{1}{2}Re\left(v\frac{\partial v}{\partial r}+u\frac{\partial v}{\partial x}\right)=-\frac{\partial P}{\partial r}+2\frac{1}{r}\frac{\partial}{\partial r}\left(\eta r\frac{\partial v}{\partial r}\right)-2\eta\frac{v}{r^2}+\frac{\partial}{\partial x}\left(\eta\left[\frac{\partial u}{\partial r}+\frac{\partial v}{\partial x}\right]\right) \quad (3)$$

$$\tfrac{1}{2}Re\left(v\frac{\partial u}{\partial r}+u\frac{\partial u}{\partial x}\right)=-\frac{\partial P}{\partial x}+\frac{1}{r}\frac{\partial}{\partial r}\left(\eta r\left[\frac{\partial u}{\partial r}+\frac{\partial v}{\partial x}\right]\right)+2\frac{\partial}{\partial x}\left(\eta\frac{\partial u}{\partial x}\right) \quad (4)$$

Energy equations

$$\tfrac{1}{2}Re\,Pr\left(v\frac{\partial\Theta_f}{\partial r}+u\frac{\partial\Theta_f}{\partial x}\right)=\frac{1}{r}\frac{\partial}{\partial r}\left(r\frac{\partial\Theta_f}{\partial r}\right)+\frac{\partial^2\Theta_f}{\partial x^2}+\tfrac{1}{2}Re\,Pr\,\eta\Theta \quad (5)$$

$$\Phi=2\left\{\left(\frac{\partial v}{\partial r}\right)^2+\left(\frac{v}{r}\right)^2+\left(\frac{\partial u}{\partial x}\right)^2\right\}+\left(\frac{\partial u}{\partial r}+\frac{\partial v}{\partial x}\right)^2 \quad (6)$$

with the following boundary conditions for the computational domain ABCDEF:

on AB,CD:

$$\frac{\partial u}{\partial r}=0,\quad v=0,\quad \frac{\partial\Theta_f}{\partial r}=0 \quad (7)$$

on AF,EF:

$$u=1,\quad v=0,\quad \Theta_f=0 \quad (8)$$

on DE:

$$\frac{\partial u}{\partial x}=\frac{\partial v}{\partial x}=\frac{\partial\Theta_f}{\partial x}=0 \quad (9)$$

on BG,HC:

$$u=v=0,\quad \frac{\partial\Theta_f}{\partial x}=0 \quad (10)$$

on GH:

$$u=v=0,\quad \frac{\partial\Theta_f}{\partial r}=0. \quad (11)$$

The boundary conditions on line segments AB and CD reflect the axisymmetric nature of the steady flow past the cylinder. On the segments AF and EF the flow conditions are taken to be free stream values since these boundaries are chosen to be far from the cylinder body. Outflow conditions are assumed to exist on the segment DE, which is located far downstream from the cylinder. At the solid–fluid interface made up of segments BG, GH and HC the no-slip condition holds along with the continuity of the interface temperature. It is also postulated that no temperature equalization occurs within the cylinder (the heat conductivity of the cylinder k_s^* is zero). This assumption has been shown to be physically reasonable in the analysis of Part I. As in Part I an average probe tip temperature, Θ_{S_p} is defined as below:

$$\Theta_{S_p}=2\int_0^1\Theta_{S|_{X=0}}r\,dr. \quad (12)$$

Constitutive equation

The constitutive equation for the Carreau model is a specific example of a generalized Newtonian fluid model in which the viscosity, η^*, is allowed to vary with the magnitude $\dot{\gamma}^*$ of the deformation rate tensor $\mathbf{D}^*$. This parameter is also commonly termed the 'shear rate' or 'deformation rate'. The most commonly used generalized Newtonian fluid model is the power law model [4, 5]. However, this simple model is not directly applicable to this type of external flow, since far from the cylinder body uniform free stream velocity conditions, and consequently zero shear rate conditions, prevail. In this case the power law model predicts a physically unrealistic infinite viscosity. For this reason, the temperature shifted Carreau or modified power law model [1], with its smooth transition to a constant viscosity at the limit of zero shear rate, is used:

$$\eta^* = \eta_0^* \frac{a_T}{[1+(\lambda_p^* a_T \dot{\gamma}^*)^2]^{(1-m)/2}}. \quad (13)$$

The two material parameters, λ_p^* and m, in the Carreau model describe the shear rate dependence of the viscosity. The power law index, m, controls the slope of the $\eta^* \propto \dot{\gamma}^{*(m-1)}$ power law region of the viscosity model, whereas the characteristic relaxation time, λ_p^*, describes the transition to a constant viscosity in the limit of zero shear rate. In this context, λ_p^* is used to describe the shear thinning behavior of the fluid; this parameter does not describe any type of viscoelastic behavior of the fluid. The above Carreau model involves the minimum number of material parameters necessary to describe the purely viscous effects which are expected to be most important in such flow situations. The study of viscoelastic effects would require a considerably more complex constitutive model and involve more material parameters; it is therefore left to later studies to detail the role of elastic effects on the viscous dissipation heating produced in such flows.

The viscosity of non-Newtonian fluids is also known to depend on temperature and pressure; the small amount of available data indicate that the temperature dependence is much stronger than the pressure dependence [1]. For this reason, the pressure dependence will be neglected in the following analysis. The temperature dependence of polymeric liquids can be described by the method of reduced variables [6] with the use of a material dependent shift factor a_T. Commonly this temperature dependence is modeled by an Arrhenius function:

$$a_T = \exp\left[\frac{E^*}{\tilde{R}^*}\left(\frac{1}{T^*} - \frac{1}{T_0^*}\right)\right]. \quad (14)$$

This relationship is observed to hold for low molecular weight fluids and molten polymers 100 K or more above their glass transition temperatures [1]. Using the definition (1) the nondimensional form of the temperature shifted Carreau model becomes:

$$\eta = \frac{a_T}{[1+(Wb\, a_T \dot{\gamma})^2]^{(1-m)/2}} \quad (15)$$

with

$$\dot{\gamma} \equiv \frac{\dot{\gamma}^* R^*}{U_0^*}$$

$$Wb \equiv \frac{\lambda_p^* U_0^*}{R^*}.$$

In this formulation the parameter Wb can be interpreted as a type of Weisenberg number describing the ratio of characteristic relaxation time of the fluid to a characteristic time, R^*/U_0^*, for the flow process. The influence of the shift factor, a_T, the Weisenberg number, Wb, and the power law index, m, is shown in Fig. 2. The nondimensional form of (14) is given by

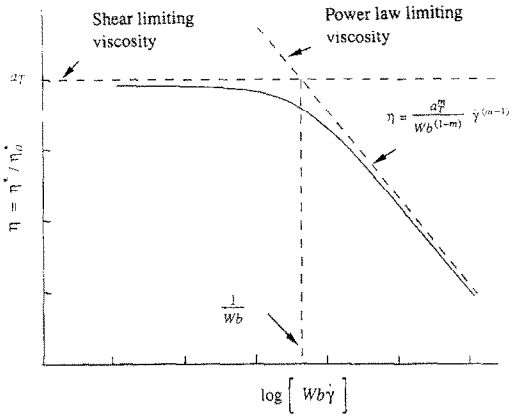

FIG. 2. Schematic diagram of temperature shifted Carreau model.

$$a_T = \exp\left(-\frac{Na\, Re}{Pr}\frac{T_0^*}{T^*}\Theta\right) \quad (16)$$

with

$$Na = \frac{\eta_0^*\left(\frac{E^*}{\tilde{R}^* T_0^{*2}}\right)U_0^{*2}}{k^*}.$$

The nondimensional parameter, Na, is the Nahme number [1, 7]. For relatively small temperature differences, $T_0^*/T^* \approx 1$, equation (16) can be simplified to

$$a_T = \exp\left(-\frac{Na\, Re}{Pr}\Theta\right), \quad (17)$$

which is assumed to describe the temperature dependence of viscosity in the analysis that follows. Winters (personal communication, 1988) indicates that equations (15) and (17) provide a good description of the temperature and shear rate dependence of viscosity for polymer melts, while at the same time eliminating the additional process-dependent parameter T_0^*/T^*. Also, it should be noted that since $T^* \geq T_0^*$, equation (17) provides an upper limit on the viscosity decreasing effect of temperature.

The nondimensional equations and boundary conditions above indicate that the dimensionless velocity, pressure and temperature fields are functions of the power law index, m, Weisenberg number, Wb, and the Nahme number, Na, for fixed Re, Pr, R^*/L^* and k_s^*/k_f^*. From the Newtonian analysis of Part I the following values, $Re = 10^{-3}$, $Pr = 10^8$, $R^*/L^* = 2.5 \times 10^{-3}$ and $k_s^*/k_f^* = 0$, have been selected as representative of such polymer flows.

COMPUTATIONAL DETAILS

The governing equations were discretized by using a control volume based finite difference scheme along

with the SIMPLER procedure for solution of the velocity and pressure fields [8]. The resulting system of nonlinear algebraic equations was linearized by a Picard iteration (or successive substitution) procedure. Thus, for example, the inherent nonlinearity of the temperature and shear rate dependence of viscosity is linearized by using values from the previous iteration to compute the viscosity at each grid point. At each iteration a direct inversion technique was used to solve for the flow variables (u, v, P), along with a line-by-line technique [8] for the temperature field Θ. A penalty method formulation is used to produce nonzero diagonal elements associated with the continuity equation in the coefficient matrix. This technique, discussed in detail in ref. [9], allows efficient inversion of the coefficient matrix using sparse matrix routines.

The computational domain was discretized by a 150×50 nonuniform grid in the x and r directions respectively. The grid was finer in the x direction at the probe tip; in the r direction the grid was finest near the probe wall GH. In order to achieve grid and domain independent results a highly nonuniform grid was found to be necessary. The details of the grid independence study can be found in Part I. The computations were performed on the Minnesota Supercomputer Institute's Cray-2 machines. Typical execution times for the numerical solutions were of the order of 600 seconds. The core memory required was about 5×10^6 Cray-2 words (64 bit words).

The influence of the nondimensional parameters on the solution of the governing equations was determined as follows. For the case of a Carreau model fluid with no temperature dependence on viscosity ($Na = 0$) the effect of the power law index, m, on the velocity and temperature fields was studied by fixing $Wb = 10^3$. The value of Wb was varied between 0 and 10^4 for $Na = 0$ and $m = 0.5$ to study its effect on the velocity and temperature fields. The effect of a temperature dependence on viscosity was studied by fixing $m = 0.5$ and $Wb = 10^3$ while varying the Nahme number from 0 to 10^4.

RESULTS AND DISCUSSION

Velocity field

The effect of the shear rate dependence of the viscosity on the hydrodynamic boundary layers around the cylinder body is presented in Fig. 3 for the case $Wb = 10^3$. The vertical and the horizontal scales in this plot are nonlinear and vary as $\sqrt{r}$ and $\sqrt{(|x - x_c|)}$ respectively. The term boundary layer in this context is used to describe the region of the flow about the cylinder body which is affected by viscous forces. In this plot the axisymmetric nature of the flow has been used in the present results for the entire plane θ = constant. It is clearly evident from Fig. 3 that a decrease in the power law index, m, causes a corresponding decrease in the thickness of the 99% boundary layer surface. Thus the non-Newtonian shear thinning behavior limits the domain influenced by the presence of the cylinder body in the uniform flow. Since m typically varies from 0.6 to 0.2 for polymer melts, it is evident that the non-Newtonian behavior has a pronounced effect on the location of the 99% boundary layer. For example, in the case of $m = 1.0$ the Newtonian boundary surface extends approximately six times further from the cylinder surface than the corresponding $m = 0.4$ surface. In Fig. 3, a 'necking' or thinning of the boundary layer surfaces near the corners of the cylinder is apparent for small values of m. This necking in the vicinity of the corners is most likely due to the existence of high shear rate regions near the corner (see Figs. 5 and 6, Part I) and the increased shear thinning of viscosity as m decreases. With this local decrease in viscosity due to shear thinning, the fluid accelerates near the corner and thereby decreases the thickness of the boundary layer.

The upstream elliptic effects due to the presence of

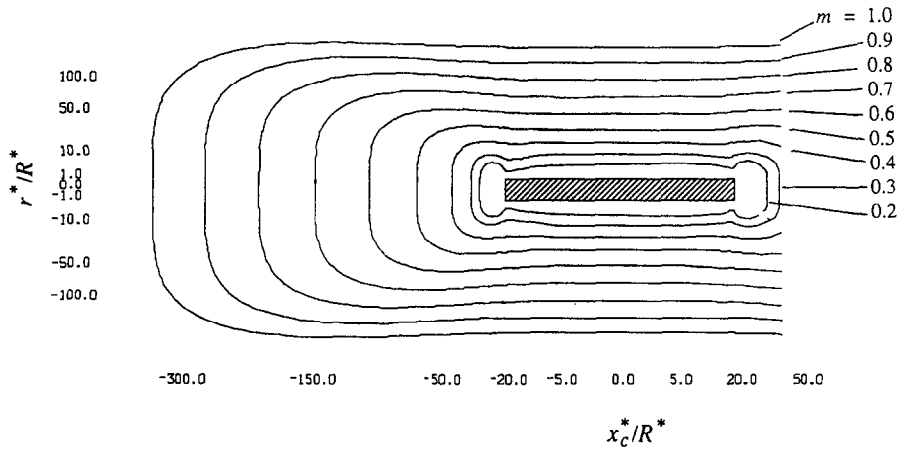

FIG. 3. Location of axisymmetric 99% boundary layer surface ($Na = 0$, $Wb = 10^3$, $u^*/U_0^* = 0.99$).

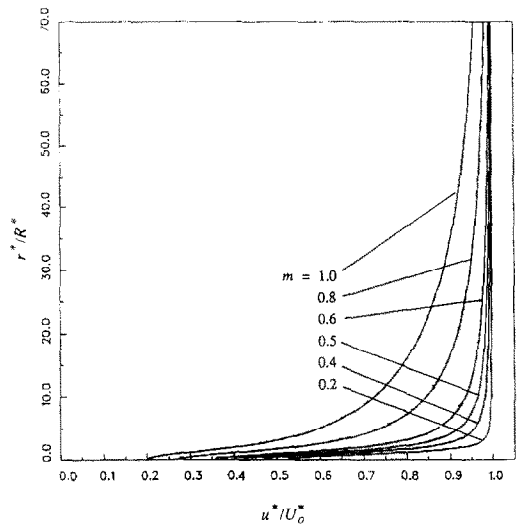

FIG. 4. Velocity profiles upstream of cylinder tip ($Na = 0$, $Wb = 10^3$, $x^*/R^* = -1.32$).

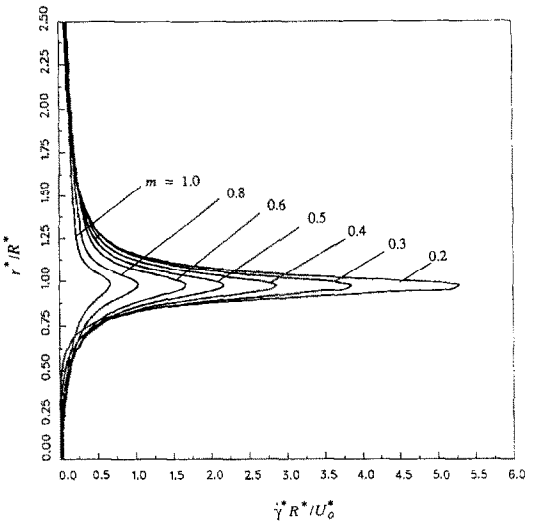

FIG. 6. Deformation rate profiles upstream of cylinder tip ($Na = 0$, $Wb = 10^3$, $x^*/R^* = -0.1$).

the cylinder body are evident in Figs. 4 and 5. In Figs. 4 and 5 nondimensional velocity profiles are plotted at a fixed point upstream of the cylinder tip. From these figures it is apparent that as the magnitude of the shear thinning effects increases, the upstream velocity profile approaches more closely a uniform flow distribution. In Fig. 5 it is evident that the influence of the Weisenberg number decreases as Wb increases to about 10^3. This trend is to be expected since as Wb increases (Fig. 2) the 'power law' region of the viscosity relationship increases in magnitude to lower shear rates. Thus in almost the entire hydrodynamic boundary layer near the cylinder body the fluid behaves as a power law type fluid.

The increase in the magnitude of the velocity gradients, and hence the deformation rate $\dot{\gamma}$, with increasing non-Newtonian behavior is most clearly seen in a plot of deformation rate just upstream of the cylinder tip. Figure 6 presents the effect of decreasing power law index, m, for a fixed $Wb = 10^3$ and $x^*/R^* = -0.10$. Clearly the local decrease in the viscosity in the high velocity gradient regions tends to further increase the magnitude of the deformation rate $\dot{\gamma}^*$. As in Part I, the maximum deformation rate is found near the corner BGH (Fig. 1) and consequently $r^*/R^* = 1.0$. The effect of decreasing m is to confine the large deformation rates to a smaller interval about $r^*/R^* = 1.0$ as well as increasing its maximum value. A similar tendency is found with increasing Weisenberg number and it is therefore not presented.

The effect of increased shear thinning behavior on the deformation rate profiles in the hydrodynamic boundary layer along the cylinder surface is presented in Figs. 7 and 8. As m decreases the boundary layer velocity profile fills out, with a corresponding decrease in the momentum deficit of the velocity profile. At the

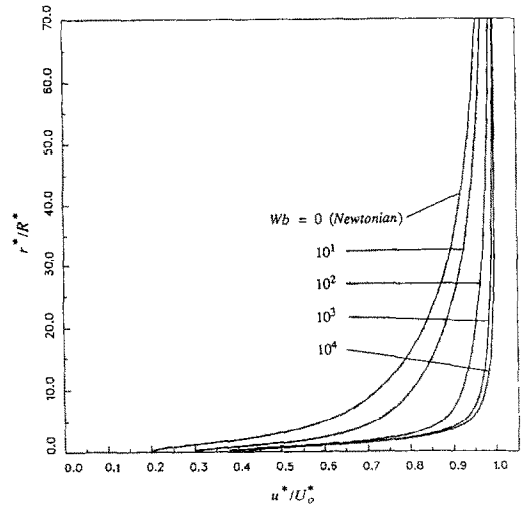

FIG. 5. Velocity profiles upstream of cylinder tip ($Na = 0$, $m = 0.5$, $x^*/R^* = -1.32$).

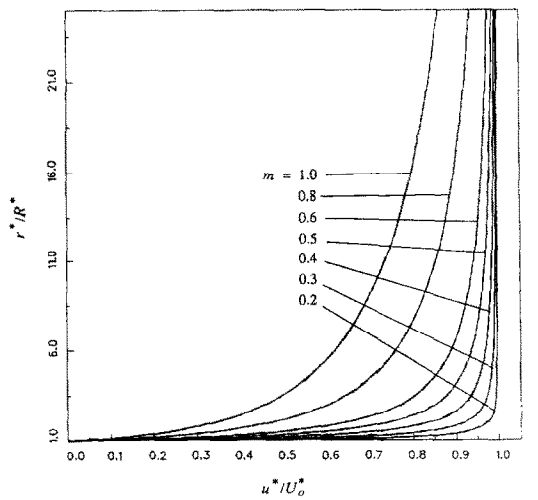

FIG. 7. Velocity profiles in hydrodynamic boundary layer on cylinder surface ($Na = 0$, $Wb = 10^3$, $x^*/R^* = 0.11$).

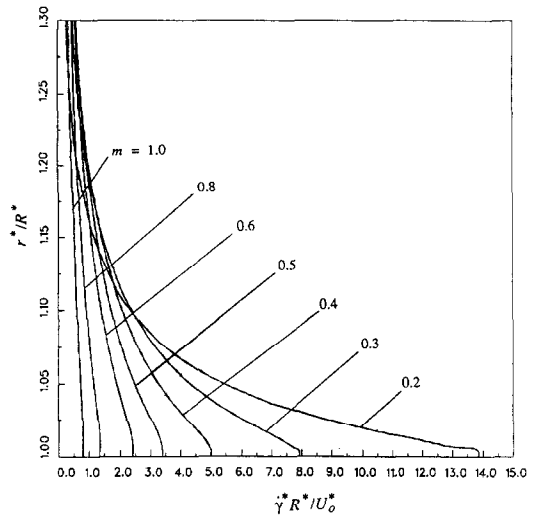

FIG. 8. Deformation rate profiles in hydrodynamic boundary layer on cylinder surface ($Na = 0$, $Wb = 10^3$, $x^*/R^* = 0.11$).

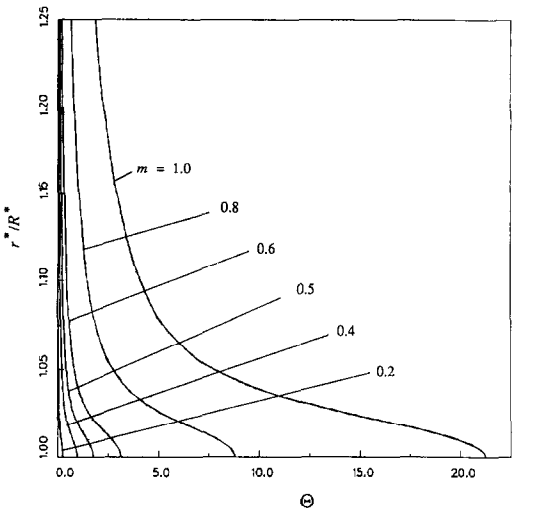

FIG. 9. Temperature profiles in thermal boundary layer on cylinder surface ($Na = 0$, $Wb = 10^3$, $x^*/R^* = 0.11$).

same time the deformation rate at the surface increases as the velocity gradient normal to the cylinder surface increases.

Temperature field

The effect of increasing non-Newtonian behavior of the Carreau model fluid on the velocity field has been summarized in the previous section. In general, as m decreases (or Wb increases) the velocity field profile fills out and the velocity gradients near the cylinder surface increase in magnitude. This increase in velocity gradient has the effect of increasing the magnitude of the viscous dissipation term (equation (6)). Counteracting this increase in velocity gradient is the corresponding decrease in the magnitude of the viscosity ratio coefficient, η, of the viscous dissipation term in equation (5). In the figures that follow it is seen that the overall effect of the increasing non-Newtonian behavior is to lower the magnitude of energy dissipated by viscous friction in the particular flow.

Figure 9 presents temperature profiles in the thermal boundary layer downstream of the cylinder tip for various values of m. In this figure, the decrease in the thermal boundary layer thickness and the adiabatic wall temperature are evident as the non-Newtonian behavior of the fluid increases. For example, a decrease in m from 1.0 to 0.4 produces a decrease of about 25 times in the local dimensionless adiabatic wall temperature. Clearly, the shear thinning effect on viscosity is an important factor in characterizing the viscous dissipation heating of such flows. The effect of increasing non-Newtonian behavior on the adiabatic wall temperature along the cylinder surface is shown in Figs. 10 and 11. From these figures, as discussed in Part I, the effect of a nonadiabatic cylinder body on the cylinder tip temperature can be estimated. However, as demonstrated in Part I, it should be possible to construct a temperature probe which behaves essentially as an adiabatic cylinder (see Fig. 13, Part I). For this reason, the effect of the increasing non-Newtonian behavior on the cylinder tip has been summarized in Figs. 12 and 13 for an adiabatic body.

Figure 12 presents the nondimensional tip temperature for various values of $0.2 \leqslant m \leqslant 1.0$ and $10^{-1} \leqslant Wb \leqslant 10^6$. A significant decrease in tip temperature is apparent in Fig. 12 for values in the range of $0.2 \leqslant m \leqslant 0.6$ and $10^1 \leqslant Wb \leqslant 10^4$ which would be representative of typical polymer melts. Also evident in Fig. 12 is a 'power law' like region for tip temperature when $10^1 \leqslant Wb \leqslant 10^5$. This region clearly corresponds to the power law asymptotic region illustrated in Fig. 2. To further demonstrate the existence of this region a power law type correlation has been fitted to the numerical data in the region, $0.2 \leqslant m \leqslant 0.8$ and $10^1 \leqslant Wb \leqslant 10^5$. The correlation given in equation (18) below is plotted with the numerical data in Fig. 13:

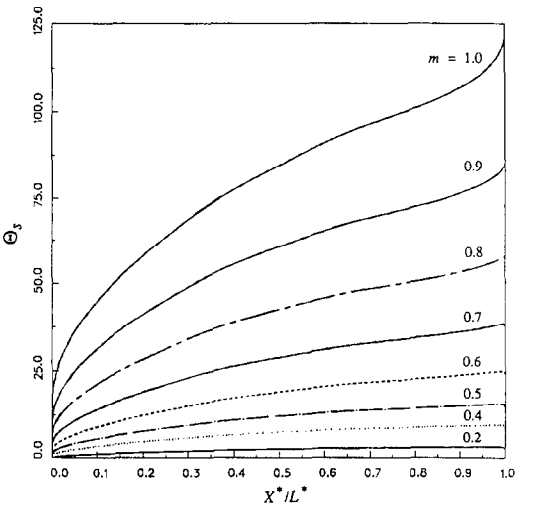

FIG. 10. Effect of power law index on local wall temperature of the cylinder ($Na = 0$, $Wb = 10^3$, $x^*/R^* = 0.11$).

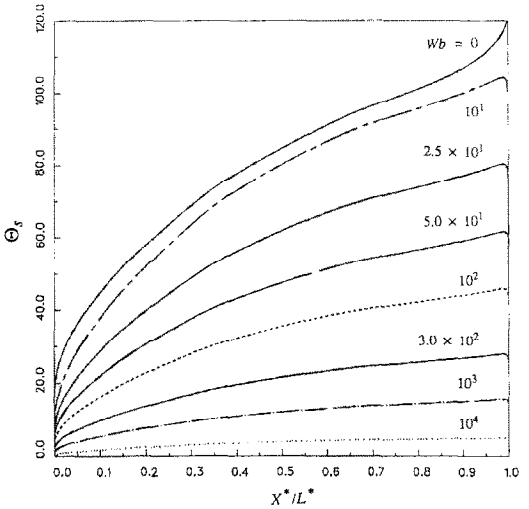

FIG. 11. Effect of Weisenberg number on local wall temperature of the cylinder ($Na = 0$, $m = 0.5$).

$$\Theta_p = 11.1(1-m)^{0.33}\, Wb^{-0.95(1-m)}. \qquad (18)$$

From Fig. 13 it is evident that the correlation is most inaccurate for $m = 0.8$ at low Weisenberg numbers and for $m = 0.2$ at higher Wb. The similarity of the slope dependence on the power law index, m, in the case of nondimensional viscosity η (equation (15) and Fig. 2) and the nondimensional adiabatic tip temperature, Θ_p (equation (18) and Fig. 13) is readily apparent.

To study the temperature dependence of viscosity

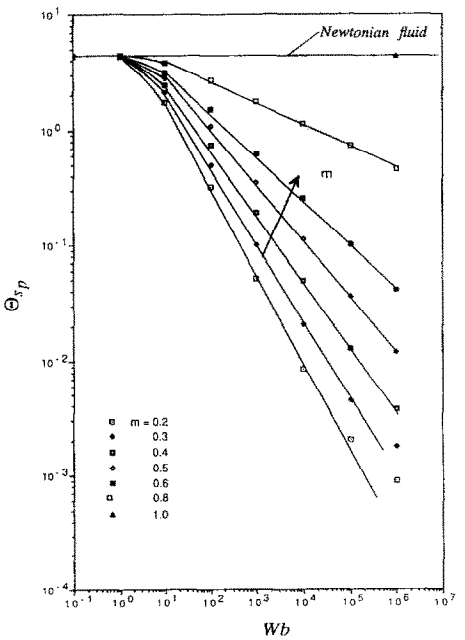

FIG. 12. Effect of Carreau model parameters on nondimensional tip temperature ($Na = 0$).

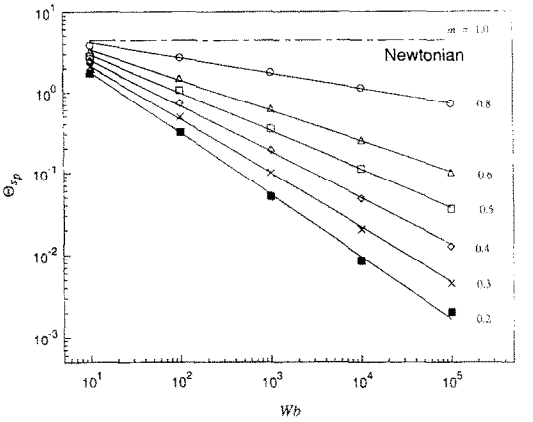

FIG. 13. Power law correlation for nondimensional tip temperature ($Na = 0$).

the Nahme number, Na, was varied from 0 to 10^4 for fixed values of Wb and m. This range is shown to be representative of the order of magnitude of the Nahme number variation by the following estimate suggested by Winter (personal communication, 1990).

Since

$$Na = \frac{[E^*/\tilde{R}^* T_0^*]U_0^{*2}}{c_p^* T_0^*} Pr \qquad (19)$$

using representative quantities:

$$Pr = 10^8, \quad c_p^* \approx 2\times 10^3 \text{ J kg}^{-1}\text{ K}^{-1},$$

$$E^* \approx 15 \text{ kcal kmol}^{-1}, \quad \tilde{R} \approx 2 \text{ kcal kmol}^{-1}\text{ K}^{-1}$$

and assuming

$$U_0^* = 0.1 \text{ m s}^{-1}, \quad T_0^* = 400 \text{ K},$$

this implies

$$Na \approx 3.75\times 10^3.$$

This establishes a reasonable range of values to study the Nahme number variation in typical polymer processing applications.

In this Nahme number range the effect of increasing temperature dependence of viscosity on the deformation rate profiles on the cylinder surface is presented in Fig. 14. These profiles are computed for $x^*/R^* = 0.11$, which is immediately downstream of the cylinder tip. It is evident that an increase in Nahme number, Na, tends to increase the wall deformation rate $\dot{\gamma}^*$. This is similar to the shear thinning effect (Fig. 8) demonstrated above, with the decrease in the local viscosity at the wall causing a corresponding increase in the velocity gradient normal to the cylinder surface. However, in this case the effect of the decrease in the local viscosity and the increase in deformation rate produce an increase in the local viscous dissipation rate. This is the opposite of the shear thinning effect which was discussed above. This increase in dissipation rate results in a higher local surface temperature as the Nahme number increases (Fig. 15).

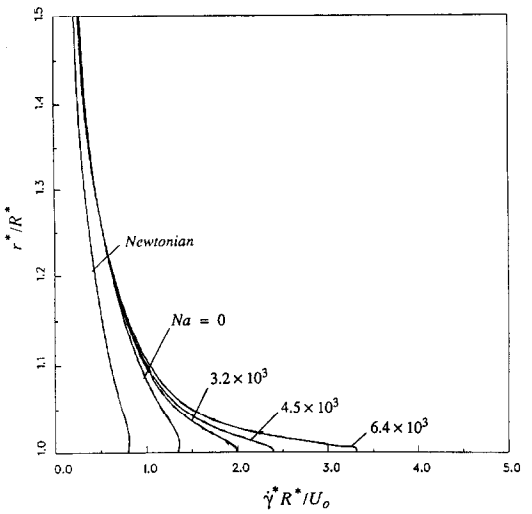

FIG. 14. Nahme number effect on deformation rate profiles in the hydrodynamic boundary layer ($m = 0.4$, $Wb = 10^4$, $x^*/R^* = 0.11$).

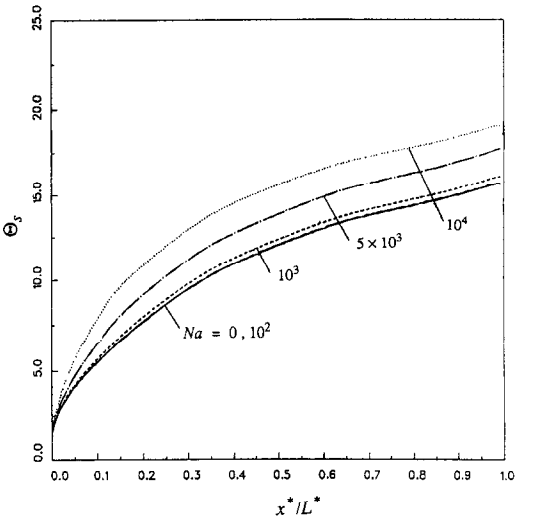

FIG. 16. Nahme number effect on the local wall temperature of the cylinder ($m = 0.5$, $Wb = 10^3$).

Apparently, the net effect of the decrease in η and the increase in $\dot{\gamma}$ (or Φ) tend to increase the viscous dissipation generation term in equation (5). The magnitude of this increase as a function of distance along the cylinder surface is shown in Fig. 16 for various values of Na. Clearly, the net effect of the temperature dependence of η is to increase the viscous heating of the cylinder surface. In contrast the temperature-dependent viscosity has very little effect on the nondimensional tip temperature for $Na \leqslant 10^4$ as presented in Table 1. From Table 1 it is apparent that for $Na \leqslant 10^4$ there is less than a 1% change in the nondimensional tip temperature. Evidently, the limited upstream elliptic influence of temperature has little effect on the temperature dependence of viscosity and hence the deformation rates local to the cylinder tip.

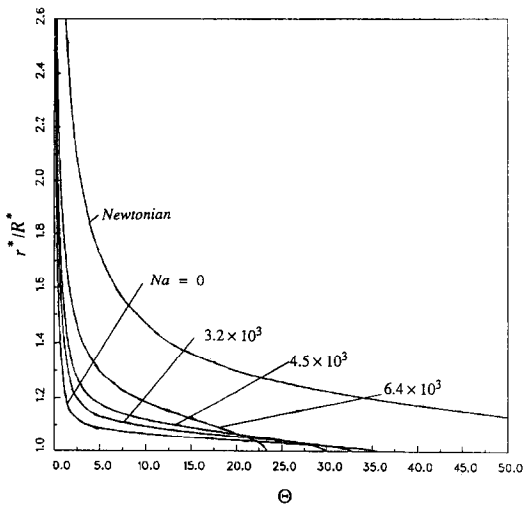

FIG. 15. Nahme number effect on temperature profiles in the hydrodynamic boundary layer ($m = 0.4$, $Wb = 10^4$, $x^*/R^* = 13.8$).

CONCLUDING REMARKS

In this study a numerical analysis has been presented for the steady, low Reynolds number flow of a high Prandtl number non-Newtonian fluid past a cylinder of finite length with its axis parallel to the main flow direction. It is thought that the cylinder approximates the shape of a temperature probe inserted into the fluid. The fluid is postulated to be a Carreau model fluid with a temperature-dependent viscosity. Part I of this study considered the limiting case of a Newtonian fluid with physical properties which are independent of temperature. In Part I the effects of Reynolds number, Prandtl number, cylinder radius to length ratio and cylinder conductivity to fluid thermal conductivity were studied. In general the results of that analysis indicated a viscosity dominated flow field with hydrodynamic boundary layers extending hundreds of cylinder radii in all directions, as well as very thin thermal boundary layers confined to narrow regions of high deformation rates near the cylinder surface. The calculations presented verified that viscous heating effects are important in such fluid flows when a temperature probe is used to measure

Table 1. Dependence of the temperature parameter Θ_{s_p} on the Nahme number ($R/L = 0.025$, $Re = 10^{-3}$ and $Pr = 10^8$, $m = 0.5$, $Wb = 10^3$)

Na	Θ_{s_p}
0.0	1.128
10^2	1.128
10^3	1.129
5×10^3	1.132
10^4	1.137

the temperature in a flowing polymer. Part II extends these results by considering the effect of a shear thinning, temperature-dependent non-Newtonian viscosity modeled by a temperature shifted Carreau fluid. This analysis presented a parametric study of the effect of shear thinning behavior, described by the power law index m and the Weisenberg number Wb, and the temperature dependence of viscosity described by the Nahme number Na. The results for a temperature-independent viscosity indicate that the magnitude of the viscous heating effect decreases substantially with increasing non-Newtonian behavior (decreasing m and/or increasing Wb). These results verified that the limiting Newtonian case studied in Part I provides an upper bound for the magnitude of the viscous dissipation heating encountered in such flows. In addition, these results revealed the existence of a power law type relationship between the non-dimensional tip temperature and the Weisenberg number and power law index. For this region a power law correlation was presented which successfully described the trend of the numerical data. The study of temperature-dependent viscosity effects indicated that in general the magnitude of the viscous dissipation heating of the cylinder surface increased with increasing Na. In addition, the results indicated a relatively small effect on the nondimensional tip temperature for the case of an adiabatic probe. Since a properly designed temperature probe should be able to approach the response of the adiabatic limit (Part I) it is concluded that the temperature dependence effect on the tip temperature is small for reasonable values of Na.

Acknowledgements—The authors would like to thank Dr H. H. Winter for his valuable comments and suggestions leading to an improved presentation of this paper. Also the help of Dr K. Kelkar with the SIMPLER algorithm and solution technique and the help of S. Olson in performing a number of the numerical runs is gratefully acknowledged. The computer time forming the basis of this research was supported by a grant from the University of Minnesota Supercomputer Institute. This work was partially supported by the U.S. Department of Energy under contract number DE-ACO4-76DP00789 at Sandia National Laboratories.

REFERENCES

1. R. C. Armstrong and H. H. Winter, Heat transfer for non-Newtonian fluids. In *Heat Exchanger Design and Data Book* (Edited by E. Schluender), pp. 2.5.12-1 1.5.2-16. Hemisphere, New York (1982).
2. E. R. G. Eckert and J. N. Shadid, Viscous heating of a cylinder with finite length by a high viscosity fluid in steady longitudinal flow—I. Newtonian fluids, *Int. J. Heat Mass Transfer* **32,** 321 334 (1989).
3. H. H. Winter, Viscous dissipation in shear flows of molten polymers. In *Advances in Heat Transfer*, pp. 205–267. Academic Press, New York (1977).
4. W. R. Schowalter, *Mechanics of Non-Newtonian Fluids*. Pergamon Press, New York (1978).
5. S. Middleman, *Fundamentals of Polymer Processing*. McGraw-Hill, New York (1977).
6. J. D. Ferry, *Viscoelastic Properties of Polymers*, 2nd Edn. Wiley, New York (1970).
7. E. R. G. Eckert and M. Faghri, Viscous heating of high Prandtl number fluids with temperature-dependent viscosity, *Int. J. Heat Mass Transfer* **29,** 1777–1183 (1986).
8. S. V. Patankar, *Numerical Heat Transfer and Fluid Flow*. Hemisphere, New York (1980).
9. M. E. Braaten, Development and evaluation of iterative and direct methods for the solution of the equations governing recirculating flows, Ph.D. Thesis, University of Minnesota (1985).

ECHAUFFEMENT VISQUEUX D'UN CYLINDRE DE LONGUEUR FINIE PAR UN LIQUIDE FORTEMENT VISQUEUX EN ECOULEMENT LONGITUDINAL PERMANENT—II. FLUIDES NON NEWTONIENS DE CARREAU

Résumé—On étudie numériquement le chauffage par dissipation visqueuse d'un cylindre de longueur finie exposé à l'écoulement permanent d'un fluide non newtonien. La solution concerne les champs de vitesse et de température elliptiques d'un fluide non newtonien de Carreau fortement visqueux autour d'un cylindre axisymétrique. Ayant en considération le traitement de polymère, la partie I de cette étude [E. R. G. Eckert et J. N. Shadid, *Int. J. Heat Mass Transfer* **32,** 321–334 (1989)] considérait l'effet des nombres de Reynolds et de Prandtl, le rapport du rayon à la longueur, et le rapport des conductivités thermiques du cylindre et du fluide. On étend ici les résultats en considérant l'effet d'une viscosité non newtonienne dépendant de la température selon le modèle de Carreau. Des calculs sont conduits pour différentes valeurs de l'exposant dans la loi puissance, des nombres de Weisenberg et de Nahme. Ces calculs sont présentés pour une éprouvette adiabatique ayant un rapport rayon sur longueur de $2{,}5 \times 10^{-2}$ et pour des nombres de Reynolds et de Prandtl respectivement fixés à 10^{-3} et 10^{8}. L'exposant varie entre 1,0 (newtonien) et 0,2, le nombre de Weisenberg entre 0 (newtonien) et 10^{4}, et le nombre de Nahme entre 0 et 10^{4}. Les résultats concernent l'accroissement des températures de la paroi et de l'extrémité dû à l'échauffement visqueux. Des effets sont sensibles pour la vitesse jusqu'à plus de 100 rayons en amont du cylindre. L'effet de la dépendance de la viscosité vis-à-vis de la température décrite par le nombre de Nahme a une faible influence sur la température de l'extrémité du cylindre.

BEHEIZUNG EINES ZYLINDERS ENDLICHER LÄNGE DURCH VISKOSE DISSIPATION BEI DER STATIONÄREN LÄNGSANSTRÖMUNG DURCH EIN FLUID GROSSER ZÄHIGKEIT—II. NICHT-NEWTON'SCHE MODELLFLUIDE NACH CARREAU

Zusammenfassung—Die Beheizung eines Zylinders endlicher Länge durch viskose Dissipation bei der gleichmäßigen stationären Anströmung durch ein Nicht-Newton'sches Fluid wird numerisch untersucht. Als Lösung ergeben sich die elliptischen Geschwindigkeits- und Temperaturfelder in einem Nicht-Newton'schen Modellfluid hoher Viskosität nach Carreau in der Umgebung eines achsensymetrischen Zylinders. Vor dem Hintergrund der Polymerverarbeitung befaßte sich Teil I dieser Untersuchung mit dem Einfluß der Reynolds-Zahl, der Prandtl-Zahl, des Verhältnisses von Radius zu Länge sowie des Verhältnisses der Wärmeleitfähigkeiten von Zylinder und Fluid. In der vorliegenden Arbeit erfolgt eine Erweiterung zur Berücksichtigung des Einflusses einer temperaturabhängigen Nicht-Newton'schen Viskosität, die unter Schubspannung abnimmt und durch ein temperaturversetztes Fluid nach Carreau dargestellt wird. Die Berechnungen wurden für unterschiedliche Werte des Exponenten im Potenzansatz, der Weisenberg-Zahl und der Nahme-Zahl durchgeführt. Die Berechnungen erfolgten für eine adiabate Probe mit einem Radius/Längen-Verhältnis von $2{,}5 \times 10^{-2}$, einer Reynolds-Zahl von 10^{-3} und einer Prandtl-Zahl von 10^{8}. Der Exponent wird zwischen 1,0 (Newton'sches Fluid) und 0,2 variiert, die Weisenberg-Zahl zwischen 0 (Newton'sches Fluid) und 10^{4} und die Nahme-Zahl zwischen 0 and 10^{4}. Die Ergebnisse zeigen den Anstieg der Temperaturen an Zylinderwand und -stirnseite aufgrund der Reibungsheizung. Es ergeben sich stark elliptische Einflüsse auf die Geschwindigkeit, die sich über eine Länge von über 100 Radien stromaufwärts des Zylinders erstrecken. Wie erwartet nimmt aufgrund der scherungsbedingt verringerten Viskosität die Stärke der Beheizung der Probenoberfläche aufgrund der viskosen Dissipation ab. Im Gegensatz dazu hat die Temperaturabhängigkeit der Viskosität (wie sie die Nahme-Zahl beschreibt) einen verhältnismäßig geringen Einfluß auf die Temperatur der Zylinderstirnfläche.

ВЯЗКОСТНЫЙ НАГРЕВ ЦИЛИНДРА КОНЕЧНОЙ ДЛИНЫ ПРИ СТАЦИОНАРНОМ ПРОДОЛЬНОМ ОБТЕКАНИИ ВЫСОКОВЯЗКОЙ ЖИДКОСТЬЮ—II. НЕНЬЮТОНОВСКИЕ ЖИДКОСТИ, ОПИСЫВАЕМЫЕ МОДЕЛЬЮ КАРРО

Аннотация—Численно анализируется нагрев за счет вязкостной диссипации цилиндра конечной длины, обтекаемого стационарным потоком неньютоновской жидкости с постоянной скоростью. Определяются эллиптическое поле, а также поля скоростей и температур в модели Карро для высоковязкой неньютоновской жидкости, обтекающей осесимметричный цилиндр. В части I настоящего исследования рассматривалось влияние чисел Рейнольдса и Прандтля, а также отношений радиуса зонда к его длине и теплопроводностей цилиндра и жидкостей в приложении к обработке полимеров. В данной части полученные результаты обобщаются на случай учета влияния зависящей от температуры аномальной сдвиговой вязкости, моделируемой жидкостью Карро с изменяющейся температурой. Расчеты проводились для различных значений показателя степенного закона, а также чисел Вайзенберга и Наме. Представлены расчеты для алиабатического зонда с отношением радиуса к длине, равным $2{,}5 \times 10^{-2}$, и числами Рейнольдса и Прандтля, составляющими соответственно 10^{-3} и 10^{-8}. Показатель степенного закона варлируется от 0,1 (ньютоновского) до 0,2; число Вайзенберга—от О (ньютоновского) до 10^{4} и число Наме—в интервале $0–10^{4}$. Результаты указывают на рост температуры стенки и вершины цилиндра за счет вязкостного нагрева. Сильное эллиптическое влияние на стеку цилиндра распространяется на длину ста радиусов вверх по течению от цилинра. Как и ожидалось, что уменьшение сдвиговой аномальной вязкости приводит к снижению величины нагрева поверхности зонда за счет вязкостной диссипации. Напротив, температурная зависимость вязкости, описываемой числом Наме, оказывает сравнительно небольшое влияние на температуру вершины цилиндра.